Astronomy & Astrophysics manuscript no. src September 13, 2011
(DOI: will be inserted by hand later)

Hard X-Ray Background of the Milky Way in its Anticenter ⋆

R. Krivonos[1,2], S. Tsygankov[1,2,3,4], M. Revnivtsev[2], S. Sazonov[2], E. Churazov[1,2], R. Sunyaev[1,2]

[1] Max-Planck-Institute für Astrophysik, Karl-Schwarzschild-Str. 1, D-85740 Garching bei München, Germany
[2] Space Research Institute, Russian Academy of Sciences, Profsoyuznaya 84/32, 117997 Moscow, Russia
[3] Finnish Centre for Astronomy with ESO (FINCA), University of Turku, Väisäläntie 20, FI-21500 Piikkiö, Finland
[4] Astronomy Division, Department of Physics, FI-90014 University of Oulu, Finland

the date of receipt and acceptance should be inserted later

Abstract. We present results of a study of the Galactic Ridge X-ray Emission (GRXE) in hard X-rays with the IBIS telescope aboard INTEGRAL in the region near the Galactic Anticenter (GA) at $l = 155^\circ$. We put a conservative 2σ upper limit on the flux from the GA in the $25 - 60$ keV energy band of 1.25×10^{-10} erg s^{-1} cm^{-2}(12.8 mCrab) per IBIS field of view, or 6.6×10^{-12} erg s^{-1} cm^{-2} deg^{-1} (0.7 mCrab deg^{-1}) per unit Galactic longitude in the $135^\circ < l < 175^\circ$ region. This upper limit exceeds by an order of magnitude the expected GRXE intensity in the GA direction, given the near-infrared (NIR) surface brightness of the Milky Way in this region and the standard hard X-ray to NIR intensity ratio for the GRXE. Therefore, the non-detection of hard X-ray emission from the GA is consistent with the stellar origin of the GRXE.

Key words. galaxy: structure – X-rays: diffuse background

1. Introduction

The stellar origin of the Galactic hard X-ray background, better known as the Galactic Ridge X-ray Emission (GRXE), has recently been strongly supported by morphological/spectral studies with the RXTE and INTEGRAL observatories (Revnivtsev et al. 2006; Krivonos et al. 2007a; Türler et al. 2010), spectral studies with Suzaku (Ebisawa et al. 2008; Yamauchi et al. 2008) and direct X-ray source counts with Chandra (Revnivtsev et al. 2009, 2011). The GRXE does not arise from the interaction of cosmic rays with the interstellar medium, as was believed before, but is associated with the (predominantly old) stellar population of the Galaxy, namely with hard X-ray emission from accreting white dwarfs and coronaly active stars. It was demonstrated (Revnivtsev et al. 2006; Krivonos et al. 2007a) that GRXE intensity closely follows near-infrared (NIR) surface brightness over the Milky Way, which is a known tracer of stellar mass.

Galactic diffuse emission in a region far away from the Galactic Center (GC) was studied by Skibo et al. (1997) using OSSE observations at longitude $l = 95^\circ$. The observed emission was suspected to contain a significant contribution from bright discrete sources due to the large collimated field of view ($\sim 11^\circ.4 \times 3^\circ.8$), but a major part of the detected flux was interpreted as interstellar emission from non-thermal electrons (see also e.g. Valinia et al. 2000; Valinia & Tatischeff 2001). Today, thanks to the unique possibilities of INTEGRAL gamma–ray telescopes, we can directly study the Galactic diffuse background in any parts of the Galaxy without dealing with significant source contamination.

Given the distribution of 4.9μm NIR intensity over the Galaxy as measured by the COBE/DIRBE experiment, the GRXE is not expected to be detectable in the Galactic Anticenter (GA) because of the low NIR surface brightness in this region. Nevertheless, an explicit demonstration of the fact that the GRXE is not observed from a Galactic region of low stellar density, such as the GA, would further substantiate the stellar paradigm of the GRXE. Furthermore, placing tight constraints on the hard X-ray flux from the GA region is important for calibrating futher studies of the GRXE in the central parts of the Galaxy.

2. Observations

This study utilizes data from the ISGRI detector, the first layer of the IBIS coded-mask telescope (Ubertini et al. 2003), aboard the INTEGRAL gamma-ray observatory

⋆ Based on observations with INTEGRAL, an ESA project with instruments and science data centre funded by ESA member states (especially the PI countries: Denmark, France, Germany, Italy, Switzerland, Spain), Czech Republic and Poland, and with the participation of Russia and the USA

(Winkler et al. 2003). ISGRI operates at energies above $\sim$ 20 keV, with the sensitivity rapidly decreasing above 100 keV. IBIS has a relatively large field of view ($\sim 28^\circ \times 28^\circ$ at zero response), which allows one to measure weak diffuse emission fluxes by using the telescope as a collimated instrument.

To study the GRXE in the GA region, we used special INTEGRAL observations, part of a series of so-called Galactic Latitude Scans (*GLS*). This program is based on consecutive observations made along the Galactic latitude in the range $\pm 30^\circ$ with a step of 2°. Such a strategy allows one to make independent snapshot measurements of the instrumental background at mid latitudes, where the GRXE is expected to be negligible, along with an actual GRXE observation near the Galactic plane. Crucially, the instrumental background, which is usually high in hard X-ray observations, does not exhibit strong variability during an individual *GLS* lasting ~ 8 hours.

There are two positions in the GA region observed with *GLS*s: on-going observations at $l = 215^\circ$ (PI: Tsygankov) and a completed program at $l = 155^\circ$ with a total exposure of 1 Ms (PI: Krivonos). In the present study we only used the completed *GLS* observations at $l = 155^\circ$ performed in August–September 2010, see Table 1 for details. Having screened the whole dataset following the procedure described in Krivonos et al. (2007a), hereafter K07, we were left with 525 out of 569 *ScW*s for subsequent scientific analysis.

To model background variations (Sect. 3.3), we used public data of high latitude observations (Table 1).

Table 1. INTEGRAL observations used for the GRXE study.

Latitude scan at $l = 155^\circ$, 2010		
Observation field	Orbits	*ScW*s
...	960,961	2–94,11–97
...	962,963	12–112,1–97
...	964,965	13–110,2–67
...	966	23–56
569 *ScW*s, total nominal exposure: 1 Ms.		
Background model calibration, 2008–2009		
Observation field	Orbits	
North Ecliptic Pole	686–689, 759–761, 824–829	
XMM-LSS	695, 696, 701	
Virgo Cluster	747–754, 758, 819–820	
Coma Cluster	821–823	
M82 X-1	869–872	
3C273, 3C279 and M87	878–880	
Total nominal exposure: 6 Ms.		
Crab calibration, 2010		
Observation field	Orbits	
Crab Nebula	902, 903, 966-968, 970	
Total nominal exposure: 890 ks.		

3. Analysis

In the present study we mainly follow the approach described in K07. Our study of the GRXE is based on the capability of the IBIS telescope to separate the contributions of point sources from the background count rate.

The ISGRI detector shadowgramm accumulated during an individual INTEGRAL observation (called *Scientific Window*, *ScW*) in a given energy range is cleaned from source fluxes using the known pattern of the IBIS mask. The remaining shadowgramm contains the variable instrumental background, assumed to be constant, the isotropic Cosmic X-ray Background (CXB, see Sect. 3.5), and the GRXE. Since the latter is extended over the sky, it cannot be directly resolved with the IBIS mask. The only way to estimate the GRXE flux is to determine the difference between the observed, clean from sources, collimated detector count rate and the assumed instrumental background. To this end, we define a background model that predicts the background count rate during a given GRXE observation. The background model is adjusted very precisely using mid-latitude snapshots of the background performed shortly before and after a given GRXE observation, which is the main concept of the *GLS*.

3.1. Detector shadowgramm

Since IBIS is a coded aperture imaging telescope, the sky is projected onto the detector plane through the transparent and opaque elements of the mask mounted above the detector plane. We produced the ISGRI detector shadowgramm for every *ScW* as described in K07. We used the $25 - 60$ keV working energy band because of the known evolution of the low-energy threshold of the ISGRI detector and since the GRXE is expected to be weak above $\sim$ 50 keV due to the high energy cut-off in the GRXE spectrum (Krivonos et al. 2007a; Revnivtsev et al. 2006).

3.2. Sky map

The sky reconstruction is based on deconvolution of the detector shadowgramm with a known mask pattern. We implemented the IBIS/ISGRI sky reconstruction method described in our previous publications (Revnivtsev et al. 2004; Krivonos et al. 2005, 2007a,b). For the basic idea we refer the reader to the papers by Fenimore & Cannon (1981) and Skinner et al. (1987). Every sky image was additionally cleaned from systematic noise as described in Krivonos et al. (2010a). The resulting sky image mosaic is shown in Fig. 1.

The survey area as a function of flux for sources with $S/N > 5$ is shown in Fig. 2. The minimum detectable flux in the central part of the field is 2.4×10^{-11} erg s^{-1} cm^{-2}(or 2.5 mCrab). The survey area reaches its geometric limit of 3650 deg^2 for $f > 4.9 \times 10^{-9}$ (500 mCrab), 50% of this area has a sensitivity better than 8.1×10^{-11} (8.3 mCrab).

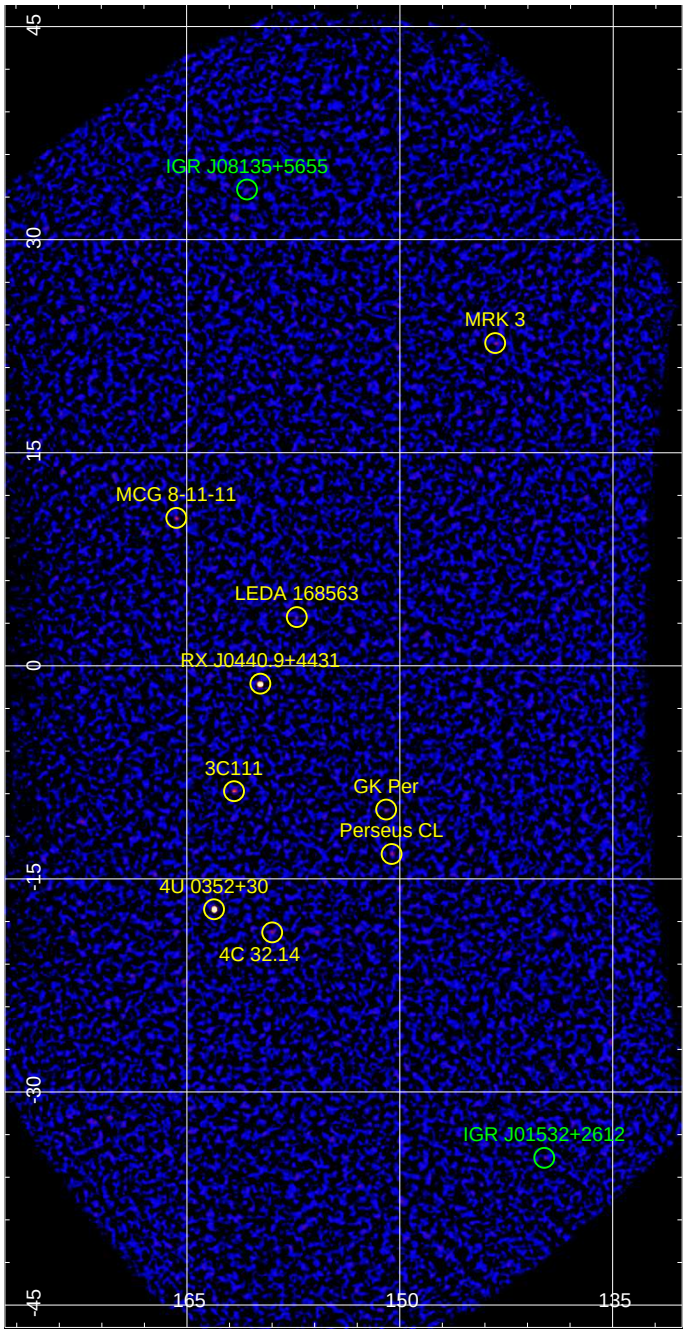

Fig. 1. IBIS/ISGRI sky image of the 1 Ms observation of the GA region at $l = 155°$ produced in the $25 - 60$ keV energy range. The image is shown in significance with a squared root color map ranging from 0 to 25. The black and blue colors correspond to pixel values from 0 to 2. The red pixels have values of around 5. The yellow to white color transition corresponds to 15 and more. The cataloged and newly detected sources are labeled in yellow and green, respectively.

We performed a search for sources as excesses in the sky mosaic (Fig. 1) convolved with a Gaussian representing the effective instrumental PSF. The detection threshold was estimated assuming gaussian noise of the pixel values as follows. The total area of the sky image (Fig. 1)

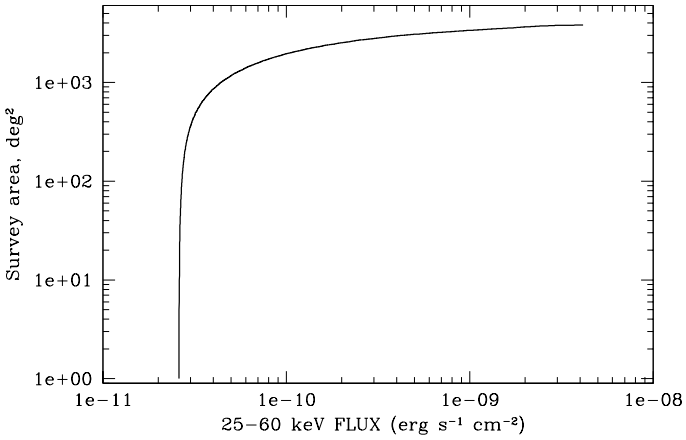

Fig. 2. Survey area as a function of flux for sources with $S/N > 5$

is 3650 squared degrees, and taking the IBIS telescope angular resolution of $12'$ into account we gather $\sim 9.12 \times 10^4$ independent pixels. With this consideration, we set the source detection threshold to 5σ allowing at most one false detection *for pure Gaussian noise*.

The signal-to-noise ratio distribution of pixels shown in Fig. 3 has the expected Gaussian shape. However, one notices some systematic excess at the negative side. Nevertheless, the source detection thereshold of 5σ, estimated above, separates the noise and source dominated pixel domains.

The list of point sources is presented in Table 2. We attribute two marginaly detected, previously unknown sources to the systematic noise. IGR J08135+5655 is not detected in the sky mosaic of the slightly broader energy band $20-60$ keV. Although IGR J01532+2612 *is* detected in the $20 - 60$ keV band, the region around the source is affected by systematic noise at the edge of the sky mosaic.

The list of sources in Table 2, except two IGR's mentioned above, was used in the source removal procedure (Iterative Source Removal, IROS) that we applied to every ISGRI detector shadowgramm (e.g. Krivonos et al. 2010a). This procedure introduces additional uncertainty to the background model (Sect. 3.4), but allows to track source variability. For example, the known Be/X-ray binary RX J0440.9+4431 (LS V +44 17) was in a strong outburst during the observations (Krivonos et al. 2010c; Tsygankov et al. 2011).

3.3. Background model

The background model used in K07 was slightly changed in this study. Since the *GLS* observations were performed over a relatively short time period, we removed the long-term time part from the equation. Instead of using the gain parameter to trace orbital modulations of the background rate, we utilized the spacecraft orbital phase P in a quadratic polynomial form. Hereafter, we consider only the detector count rates after removal of the contribution

Table 2. The list of sources significantly ($\geq 5\sigma$) detected on the sky mosaic (Fig. 1). The newly detected sources are highlighted in bold. The 68% confidence interval for estimated sky coordinates depends on source significance: 2.1′, 1.5′, and $< 0.8'$for $5-6$,10, and $> 20\sigma$, respectively (Krivonos et al. 2007b)

Name	lon. deg.	lat. deg.	$F_{25-60\ \mathrm{keV}}$ mCrab	sign.	Type	Notes
4U 0352+30	163.08	-17.14	39.42 ± 0.69	57.33	HMXB	
RX J0440.9+4431	159.82	-1.26	26.12 ± 0.53	48.82	HMXB	
3C111	161.68	-8.83	5.32 ± 0.60	8.84	AGN	z(∼) 0.0485
MCG 8-11-11	165.74	10.41	7.27 ± 0.86	8.41	AGN	z(∼) 0.02004
4C 32.14	158.99	-18.77	3.15 ± 0.56	5.63	QSO	z(∼) 1.258497
LEDA 168563	157.26	3.43	2.76 ± 0.49	5.58	AGN	z(∼) 0.029
MRK 3	143.29	22.72	7.23 ± 1.33	5.43	AGN	z(∼) 0.013443
Perseus CL	150.58	-13.25	3.06 ± 0.58	5.30	Cluster	z(∼) 0.0179
IGR J01532+2612	139.82	-34.64	20.31 ± 3.91	5.19		
IGR J08135+5655	160.75	33.53	7.09 ± 1.38	5.14		
GK Per	150.96	-10.12	2.82 ± 0.56	5.07	CV	470 pc

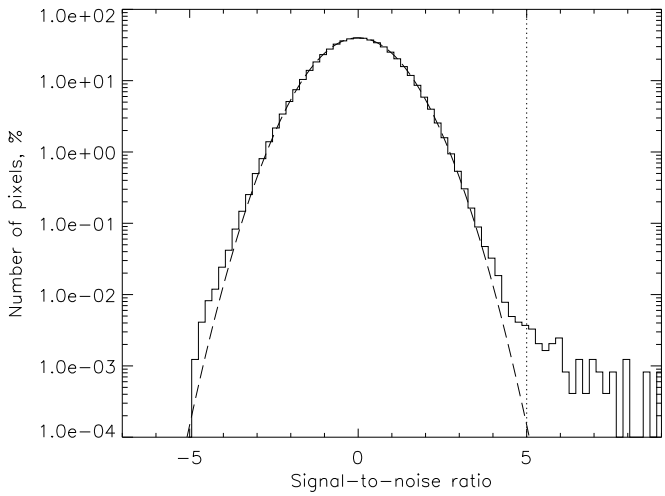

Fig. 3. Signal-to-noise ratio distribution of pixels in the 1 Ms *GLS* observation at $l = 155°$. The dashed line represents the normal distribution with unit variance and zero mean. The accepted threshold of source detection (5σ) is shown by the dotted line. The plot is truncated at $\sigma = 9$ for convenience.

of point sources. The model of the detector background $25-60$ keV count rate, D_{bgd}, is made of a linear combination of the $600-1000$ keV detector count rate, H, and phase:

$$D_{bgd} = const + aH + b_1 P + b_2 P^2 \qquad (1)$$

The coefficient a was calculated using observations pointed away from the Galactic plane ($|b| > 20°$) where the GRXE is not expected to be observed (see Table 1). The constant term and b coefficients were determined individually for each spacecraft orbit from the observations at $|b| > 20°$, thus adjusting the model to the current background level. Finding the difference between the observed and predicted by Eq. 1 detector count rates (residuals) should yield the GRXE excess in the Galactic plane.

The detector count rate was converted to the convenient units of Crab flux, with 1 mCrab $= 7.25 \times 10^{-6}$ cts/s in the $25-60$ keV band per IBIS FOV. The conversion coefficient was determined from observations of the Crab Nebula in 2010 (Table 1). A flux of 1 mCrab in the $25-60$ keV energy band corresponds to 9.7×10^{-12} erg s^{-1} cm^{-2} for a source with a Crab-like spectrum, $10.0 \times E_{\mathrm{keV}}^{-2.1}$ phot cm^{-2} s^{-1} keV^{-1}.

3.4. Model uncertainty

The uncertaity of the background model, i.e. the accuracy of the ISGRI background rate prediction, is subject to statistical and systematical errors. The former can be easily estimated from the total number of counts ($\sim 3 \times 10^5$) in the $25-60$ keV energy band per typical ScW (~ 2 ks).

The additional statistical effect is related to the IROS procedure, when the count rate attributed to a given source is removed from the detector using the known aperture function of the mask. To a first approximation, the total number of counts, S, associated with a given source is determined as the difference between the number of counts, D_1, in the detector pixels illuminated by the source through the mask and the number of counts, D_0, in the detector pixels blocked by the mask: $S = D_1 - D_0$. The total flux on the detector is $D = D_0 + D_1$. Thus, subtracting the contribution of the source yields the residual detector flux $D' = D - S = 2D_0$. For a weak source in the center of the field of view, $D_0 \approx D_1 \approx 1/2 \times D$ and therefore the relative statistical uncertainty of measuring the detector count rate $\frac{D'}{\sqrt{2D_0}} = \sqrt{2}\frac{D}{\sqrt{D}}$ increases by a factor of $\sqrt{2}$. In practice, a more complicated model of a point source (see K07), implemented in the source subtraction algorithm, causes an even larger increase of statistical uncertainties.

To estimate the IROS induced uncertainty as a function of number of sources in the FOV, we studied a set of 22 consecutive observations without catalogued and detected sources in the FOV (orbit 973, ScWs $58-80$). The relative standard deviation of detector count rate, as a function of the number of fake sources, N_{src}, in the

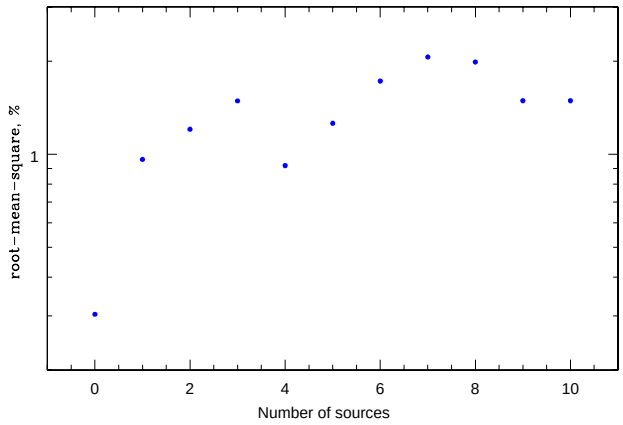

Fig. 4. Relative root-mean-squared value of the detector rate as a function of number of sources in the FOV.

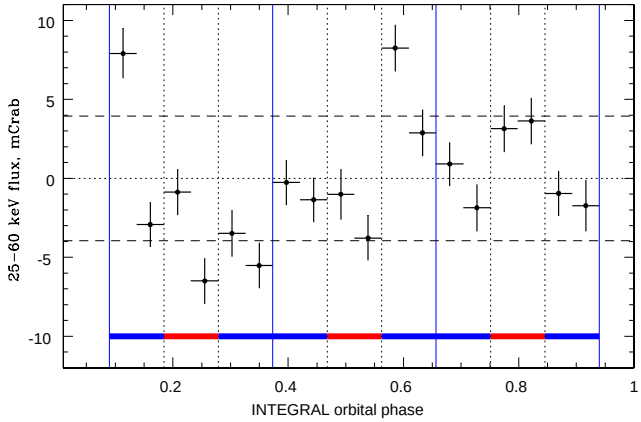

Fig. 5. Residuals after subtracting the model-predicted count rate from the observed count rate, averaged over spacecraft orbital phase. The black dashed lines represent a 1σ deviation (4.0 mCrab) of the averaged values from zero. See Sect. 3.4 for details.

FOV, is shown in Fig 4. The first point at $N_{src} = 0$, $RMS = 0.3\%$, reflects the relative statistical scatter of the data (see also Sect. 3.6). As seen from Fig 4, the scatter rapidly increases with inclusion of sources in the FOV. A typical scatter of $\sim$ 1.0% on the ScW time scale is observed in real data, as demonstrated in Sect. 4.

To estimate the systematic uncertainty of the method, we defined coefficients of the background model in Eq. 1 using the high-latitude observations (see Table 1) in the South Galactic hemisphere (700 ks) and applied it to the North (5.3 Ms). The non-existent GRXE flux was averaged over a given INTEGRAL orbit divided into three equal intervals, each having three parts: one in the middle and two adjacent, see Fig. 5 for reference. The middle part of each interval (in red) was supposed to have GRXE flux, and the neighboring parts (in blue) were used to correct the constant term (Eq.1). This set-up mimics the *GLS* pattern of observations.

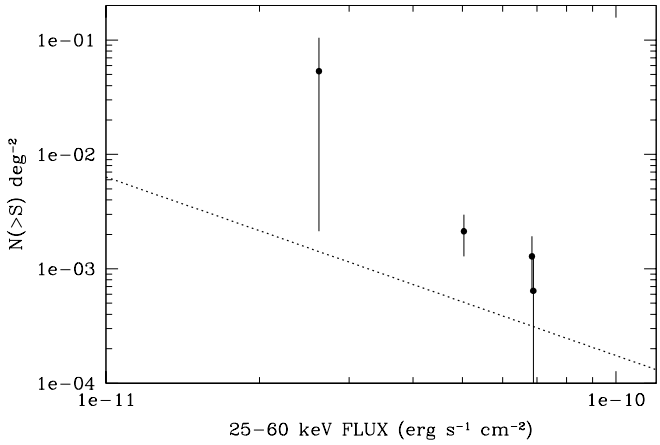

Fig. 6. Number–flux relation for non-blazar extragalactic objects detected in the survey. The dotted line represents the $\log N$–$\log S$ relation from Krivonos et al. (2010b).

The standard deviation of residuals from zero represents the systematic uncertainty of our background model, which is found to be $\sim$ 4.0 mCrab. The $25-60$ keV detector count rate raised from $\sim$ 2.2 to $\sim$ 2.5 Crab over the considered time period, hence the relative accuracy of the model is $\sim$ 0.17% of the observed background rate.

3.5. CXB cosmic variance

Throughout the analysis we assumed the CXB flux to be constant and isotropic. However, the CXB emission coming from the population of unresolved extragalactic sources (active galactic nuclei, AGNs) is subject to Poissonian variations in the number of sources, intrinsic source variability, and nearby large-scale structure (see e.g. Fabian & Barcons 1992). Here, we estimate the systematic limitations to the measured GRXE flux caused by CXB variations.

During the GA survey we detected an enhanced number of extragalactic sources: four nearby AGNs, a QSO and a cluster of galaxies (see Table 2). Fig. 6 shows the number-flux relation of the detected AGNs in comparison with the best-fit $\log N$–$\log S$ function of 158 non-blazar AGNs derived over the extragalactic sky ($b > 5^\circ$) in the 7-year INTEGRAL survey (Krivonos et al. 2010b). This $\log N$–$\log S$ relation was converted from $17-60$ keV to $25-60$ keV assuming a power-law spectrum with a slope of 1.8.

Using the extragalactic $\log N$–$\log S$ relation from Krivonos et al. (2010b) and following Revnivtsev et al. (2008), we estimated the relative uncertainty of the CXB flux in the $25-60$ keV band as:

$$\left(\frac{\delta I_{CXB}}{I_{CXB}}\right)_{\Omega} \sim 5.5\times10^{-2} S_{\rm max,11}^{1/4}\Omega_{\rm deg}^{-1/2}. \qquad (2)$$

where $S_{\rm max,11}$ is the maximal flux of undetected sources in units of 10^{-11} erg s^{-1} cm^{-2}, and $\Omega_{\rm deg}$ is the solid angle of the instrument's field of view. We adopted the CXB inten-

sity to be equal to 1.89×10^{-11} erg s^{-1} cm^{-2} deg^{-2}, based on the CXB spectrum model of Gruber et al. (1999) and the $\sim 10\%$ higher normalization measured by INTEGRAL (Churazov et al. 2007). Using the limiting flux of the survey and effective solid angle of the IBIS telescope (~ 286 deg^2), Eq. 2 yields a CXB variance at the level of $\sim 0.4\%$, or 2.3 mCrab assuming a $\sim$ 550 mCrab CXB flux per IBIS FOV. Below, we also consider the CXB variance for an area of three IBIS FOVs, which approximately corresponds to the effective area of the GA survey.

3.6. Summary of uncertainties

We now summarize all the discussed uncertainties related to the GRXE measurements in the $25 - 60$ keV energy band. The uncertainties below are presented with respect to the background rate, which is assumed to be 2.5 Crab. *Statistical uncertainties:*

- 0.18% (4.5 mCrab) – count statistics, *expected* for 3×10^5 counts per typical ScW ($\sim$ 2 ks),
- 0.30% (7.5 mCrab) – count statistics, *observed* in a typical ScW without any sources in the FOV. Since this value differs from the expected, it cannot be fully statistical. Some unexplored systematics or background variability can contribute to the scatter of the observed detector count rate.
- 1.00% (25 mCrab) – observed in a typical ScW with several sources in the FOV, related to the IROS procedure.

These uncertainties constitute the error of measurement and, naturally, decrease with increasing exposure. For example, the largest error of 25 mCrab decreases to 1 mCrab for a total exposure of 1 Ms. *Systematic uncertainties:*

- 0.16% (4.0 mCrab) – root-mean-squared residuals after background model subtraction from the observed count rate (Fig. 5),
- 0.09% (2.3 mCrab) – CXB variance per IBIS FOV,
- 0.16% (4.0 mCrab) – CXB variance per GA survey area.

The systematics quadratically add to the error of the measurement. The total systematic error owing to the background model and CXB variance (per GA survey area) is 5.7 mCrab.

4. Results

Using the method described above, we obtained for each *ScW* the detector count rate left after subtraction of the contribution of point sources and the predicted detector background. In Fig. 7 we show typical observed and predicted detector light curves during a spacecraft orbit. Similar to Fig. 5, we denoted regions of background measurement ($|b| >= 20°$) in blue, and actual GRXE observations in red ($|b| < 20°$). Fig. 7 demonstrates that the background behavior in an individual orbit can be captured only with fast scanning observations such as *GLS*s.

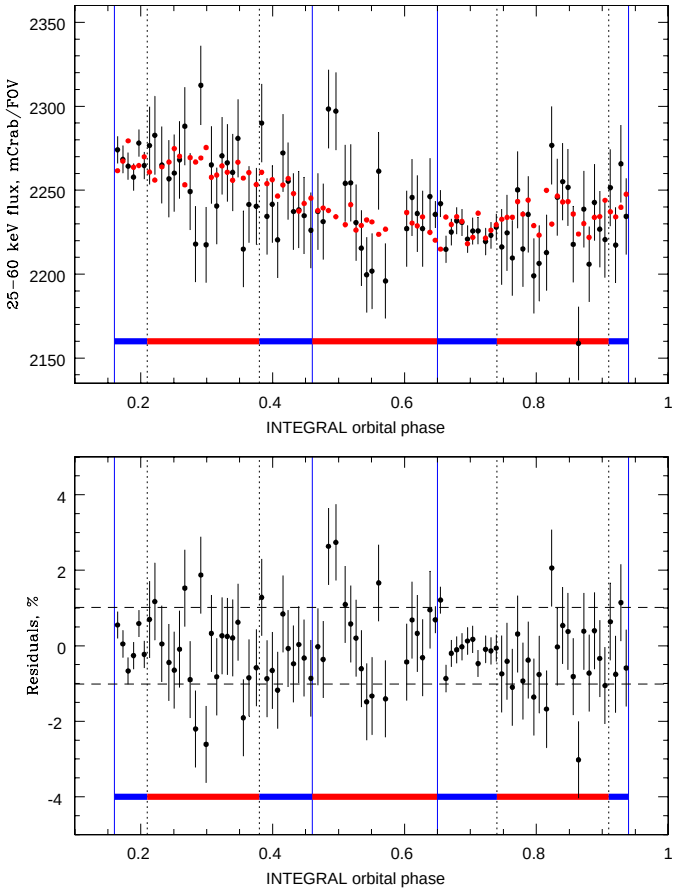

Fig. 7. *Upper panel:* Detector count rate (black) of the individual *ScW*s during orbit 964. The systematic uncertainty of the source removal procedure (Fig. 4) was added to the statistical errors of each point. The red points represent the count rate predicted by the background model. The blue and red areas denote observations made at $|b| >= 20°$ and $|b| < 20°$, respectively. *Bottom panel:* Residuals after subtracting the model-predicted count rate from the observed count rate. The black dashed lines represent a 1σ deviation (1.02%) from zero.

The background model, with low intrinsic scatter, exactly follows the observed detector rate, and the scatter of residuals (lower panel of Fig. 7) is comparable to the statistical uncertainty of $\sim 1.0\%$ associated with the IROS procedure (Sect. 3.4).

Using the entire *GLS* data set at $l = 155°$, we averaged residuals over Galactic latitude, as shown in Fig. 8 by red points. The latitude profile does not demonstrate any significant excess in the Galactic plane region at $l = 0°$. As expected, the GRXE associated with the old stellar population is not detected in the GA. the 1σ upper limit on the GRXE flux in the $|b| < 5°$ latitude range, which roughly corresponds to the IBIS fully coded FOV, is $\sim$ 2.8 mCrab, or $\sim$ 6.4 mCrab taking the systematic uncertainties into account. We later refer to a 2σ upper limit of $\sim$ 12.8 mCrab.

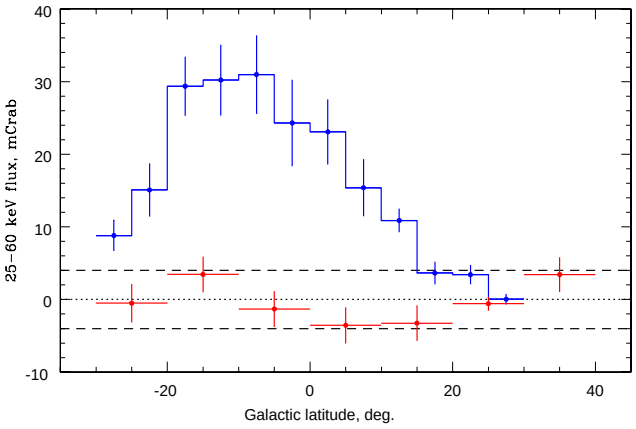

Fig. 8. Source contribution (blue) and ISGRI detector background count rate residuals (red) averaged over the Galactic latitude. Error bars of the blue histogram represent rms-deviations of the summed point source fluxes from average in bin.

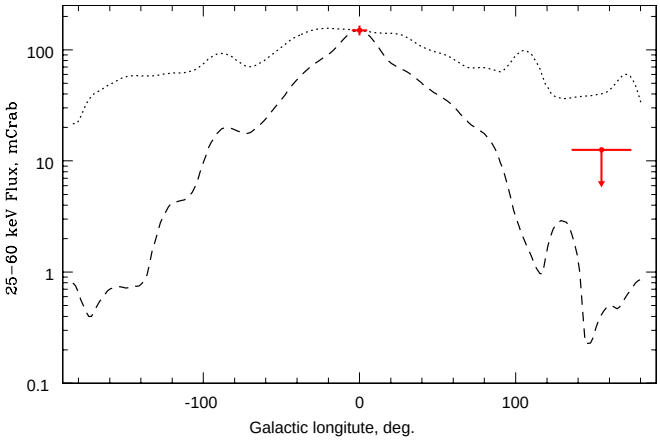

Fig. 9. Galactic longitude profiles of the COBE/DIRBE 4.9μm intensity (dashed line) and EGRET background above 100 MeV (dotted line), both normalized to the GRXE flux of 150 mCrab (red point) in the GC. The 2σ upper limit corresponds to the GRXE measurement at $l = 155°$ in the present study.

We can convert the achieved upper limit of $\sim$ 12.8 mCrab per IBIS FOV to more convenient units using the effective solid angle of the IBIS telescope ~ 286 deg^2 and taking into account that the GRXE is actually much less extended in the Galactic latitude direction than the IBIS FOV. For instance, the 2σ upper limit on the GRXE flux at $l = 155°$ per unit Galactic longitude is 0.7 mCrab deg^{-1}.

We can test the GRXE non-detection in the GA for consistency with stellar and truly diffuse GRXE origins. To this end, we compare the observed drop of the hard X-ray flux from the GC to the GA region (per IBIS FOV) with the corresponding change of the intensity of a given tracer. We use the COBE/DIRBE 4.9μm data[1] as a tracer of stellar mass, and the EGRET gamma-ray background map above 100 MeV as a tracer of the cosmic-ray induced gamma-ray background. The EGRET background intensity drops from the GC to the GA by a factor of ~ 3. Therefore, using the conservative estimate of the GRXE flux in the GC from K07 of 150 ± 15 mCrab, we expect the corresponding flux from the GA to be ~ 50 mCrab. This is definitely not observed according to Fig. 8. In contrast, there is a factor of 270 drop in the NIR 4.9μm intensity from 2.7×10^{-5} erg s^{-1} cm^{-2} to 10^{-7} erg s^{-1} cm^{-2}. This implies a GRXE flux from the GA of 0.4 mCrab at $25 - 60$ keV, which is consistent with the derived upper limit of 12.8 mCrab. This consideration is illustrated in Fig. 9, where the COBE/DIRBE and EGRET longitude profiles are renormalized to the hard X-ray flux observed from the GC. We conclude that the non-detection of the GRXE from the GA is consistent with the stellar mass distribution of the Galaxy traced by NIR maps, rather than with the cosmic-ray induced gamma-ray background seen by EGRET.

[1] COBE/DIRBE 4.9μm intensity map was corrected for the interstellar reddening and mean background level measured in high-latitude regions, as described in K07.

5. Conclusions

1) Using the 1 Ms observations of the GA at $l = 155°$ with the INTEGRAL observatory, performed in the special *GLS* mode, we did not detect the GRXE in the $25 - 60$ keV energy band and put a conservative 2σ upper limit of 1.25×10^{-10} erg s^{-1} cm^{-2}(12.8 mCrab) per IBIS FOV or 6.6×10^{-12} erg s^{-1} cm^{-2} deg^{-1} (0.7 mCrab deg^{-1}) per unit Galactic longitude.

2) The obtained upper limit is consistent with the large drop in the NIR (4.9μ) intensity observed by COBE/DIRBE and disagrees with the much smaller decrease in the gamma-ray (above 100 MeV) background measured by EGRET. Therefore, the non-detection of the GRXE in the GA is consistent with the stellar mass distribution in the Galaxy.

3) The developed background model potentialy allows us to reach the statisticaly limited accuracy. However, the final uncertainty of the approach is associated with the source removal procedure, the systematic uncertainty of the method itself, and the CXB variance. Nevertheless, the implemented method, along with the special *GLS* mode of observation, is an optimal approach of modelling the ISGRI background and can be efficiently used for studying the Galactic hard X-ray background.

4) The GA can be used to calibrate background models for studying the GRXE in the central parts of the Galaxy.

Acknowledgements. This research was done thanks to the unique capabilities of the INTEGRAL observatory. The data used were obtained from the European and Russian INTEGRAL Science Data Centers and from the High Energy Astrophysics Science Archive Research Center Online Service

of the NASA/Goddard Space Flight Center. We acknowledge the use of the Legacy Archive for Microwave Background Data Analysis (LAMBDA). Support for LAMBDA is provided by the NASA Office of Space Science. The work was supported by the President of the Russian Federation (through the program of support of leading scientific schools, project NSH-5069.2010.2), by the Presidium of the Russian Academy of Sciences/RAS (the program "Origin, Structure, and Evolution of Objects of the Universe"), by the Division of Physical Sciences of the RAS (the program "Extended objects in the Universe", OFN-16), by the Russian Basic Research Foundation (grant 10-02-00492-A), State contract 14.740.11.0611, and the Academy of Finland grant 127512.

References

Churazov, E., et al. 2007, A&A, 467, 529
Ebisawa, K., et al. 2008, PASJ, 60, 223
Fabian, A. C., & Barcons, X. 1992, ARA&A, 30, 429
Fenimore, E. E., Cannon T. M., 1981 Applied Optics, 20, 1858.
Skinner, G. K., Ponman, T. J., Hammersley, A. P., & Eyles, C. J. 1987, Astroph.Sp.Sci., 136, 337
Gruber, D. E., Matteson, J. L., Peterson, L. E., & Jung, G. V. 1999, ApJ, 520, 124
Hajdas W., Bühler P., Eggel C., Favre P., Mchedlishvili A., Zehnder A., 2003, A&A, 411, L43
Krivonos, R., Vikhlinin, A., Churazov, E., Lutovinov, A., Molkov, S., & Sunyaev, R. 2005, ApJ, 625, 89
Krivonos, R., Revnivtsev, M., Churazov, E., Sazonov, S., Grebenev, S., & Sunyaev, R. 2007, A&A, 463, 957
Krivonos, R., Revnivtsev, M., Lutovinov, A., Sazonov, S., Churazov, E., & Sunyaev, R. 2007, A&A, 475, 775
Krivonos, R., Revnivtsev, M., Tsygankov, S., Sazonov, S., Vikhlinin, A., Pavlinsky, M., Churazov, E., & Sunyaev, R. 2010a, A&A, 519, A107
Krivonos, R., Tsygankov, S., Revnivtsev, M., Grebenev, S., Churazov, E., & Sunyaev, R. 2010b, A&A, 523, A61
Krivonos, R., Tsygankov, S., Lutovinov, A., Turler, M., & Bozzo, E. 2010c, The Astronomer's Telegram, 2828, 1
Revnivtsev, M., Sunyaev, R., Varshalovich, D., et al. 2004, Astronomy Letters, 30, 382
Revnivtsev, M., Sazonov, S., Gilfanov, M., Churazov, E., & Sunyaev, R. 2006, A&A, 452, 169
Revnivtsev, M., Molkov, S., & Sazonov, S. 2008, A&A, 483, 425
Revnivtsev, M., Sazonov, S., Churazov, E., Forman, W., Vikhlinin, A., & Sunyaev, R. 2009, Nature, 458, 1142
Revnivtsev, M., Sazonov, S., Forman, W., Churazov, E., & Sunyaev, R. 2011, MNRAS, 414, 495
Skibo, J. G., et al. 1997, ApJ, 483, L95
Tsygankov, S., Krivonos, R., Lutovinov, A., 2011, MNRAS, submitted
Türler, M., Chernyakova, M., Courvoisier, T. J.-L., Lubiński, P., Neronov, A., Produit, N., & Walter, R. 2010, A&A, 512, A49
Ubertini P., et al., 2003, A&A, 411, L131
Valinia, A., Kinzer, R. L., & Marshall, F. E. 2000, ApJ, 534, 277
Valinia, A., & Tatischeff, V. 2001, Exploring the Gamma-Ray Universe, 459, 153
Winkler C., et al., 2003, A&A, 411, L1
Yamauchi, S., Ebisawa, K., Tanaka, Y., Koyama, K., Matsumoto, H., Yamasaki, N. Y., Takahashi, H., & Ezoe, Y. 2008, arXiv:0810.0317